Available online at www.sciencedirect.com
ScienceDirect
Ceramics International 34 (2008) 1503–1507
CERAMICS INTERNATIONAL
www.elsevier.com/locate/ceramint

Phase composition and properties of solid solutions of $GdFeO_3$–$GdInO_3$ bulks

D.H. Kuo [1,*], K.C. Huang

Department of Materials Science and Engineering, National Dong Hwa University, Shoufeng, Hualien, Taiwan

Received 6 February 2007; received in revised form 25 March 2007; accepted 22 April 2007
Available online 2 June 2007

Abstract

Solid solutions of the $GdFeO_3$–$GdInO_3$ system were prepared at 1550 °C by ceramic powder processing. The formulated composition was $Gd(Fe_{1-x}In_x)O_3$ (GFI) with the indium contents at $x = 0$, 0.25, 0.5, 0.75, and 1.0. A stable phase of $Gd(Fe_{1/3}In_{2/3})O_3$ in our system was identified by X-ray diffraction and phase composition analysis. Multi-phase morphologies were observed for GFI bulks with $x = 0.5$ and 0.75. Dielectric and electrical properties of the GFI bulks were investigated. The addition of 25% In^{3+} in $GdFeO_3$ had an obvious enhancement in polarization and led to an elevated resonance frequency. Dielectric properties of GFI bulks except $GdInO_3$ were strongly dependent upon the test frequency, which corresponded to the response of polarization mechanism. $GdInO_3$ displayed as a stable dielectric, which was frequency- and temperature-insensitive. $GdInO_3$ was thermally activated and became leaky until above 600 °C.

Keywords: A. Sintering; B. Microstructure-final; C. Dielectric properties; C. Electrical properties; $GdFeO_3$

1. Introduction

Rare-earth orthoferrites ($RFeO_3$, R = rare earth) are antiferromagnetic with weak superboard ferromagnetism and are of both scientific and technical interest in optic-magneto storage logic events, memory-based devices and other related applications [1,2]. Rare-earth orthoferrites have a perovskite (ABO_3) structure, which is usually distorted from the cubic to orthorhombic form with space group *Pbnm* or the $GdFeO_3$ (GFO)-type form, and are uniaxial with orthorhombic *c*-axis magnetically favored [3]. There are also tetragonal, rhombohedral, monoclinic, and triclinic perovskites which are originated from the structure deviations of the ideal cubic structure through the tilting of the BO_6 octahedra [4]. Even greater deviations can lead to a structure with hexagonal $P6_3cm$ crystallography. Other $GdFeO_3$-type compounds are RMO_3, where M represents elements of Mn, Fe, Cr, Al, Ga, V, Ti, etc. [3]. Instead of rare-earth orthoferrites, $BiFeO_3$ has been the most studied multiferroic material. Initially suffering a problem of high leakage current to inhibit ferroelectricity, $BiFeO_3$ films have improved performance by fabricating thin films with different epitaxial heterostructures [5] or on different buffered substrates [6,7]. Chemical substitutions on A or B sites of the ABO_3 perovskite structure with isovalent or aliovalent ions have been the most studied area in property modifications. $(Bi_{0.7}Ba_{0.3})(Fe_{0.7}Ti_{0.3})O_3$ films and Cr-doped, Ti^{4+} donor-doped, and La-doped $BiFeO_3$ films have been investigated with improved performance [8–11].

$GdInO_3$ has a perovskite structure with the hexagonal $P6_3cm$ crystallography [12]. Contributed from oxygen conductivity, $GdInO_3$ has a potential to be used as the electrolyte of solid oxide fuel cells. Based upon our preliminary experiments, it was observed that $GdInO_3$ dissolved into $GdFeO_3$ to a large degree. Therefore, the solid solution of the orthorhombic $GdFeO_3$-hexagonal $GdInO_3$ system aroused our interests in investigating their phase composition and properties. This system was prepared based upon the chemical formula of $Gd(Fe_{1-x}In_x)O_3$ with $x = 0$, 0.25, 0.5, 0.75, and 1.0 or abbreviated as GFI-*x*.

2. Experimental

GFI bulks were prepared by a conventional ceramic route. Gd_2O_3, In_2O_3, and Fe_2O_3 ceramic powders were the raw

* Corresponding author.
E-mail address: dhkuo@mail.ntust.edu.tw (D.H. Kuo).
[1] Present address (as of 1st August 2007): Department of Polymer Engineering, National Taiwan University of Science and Technology, Taipei, Taiwan.

0272-8842/$34.00
doi:10.1016/j.ceramint.2007.04.016

materials. After mixing powders according to the formulated composition, the mixture was firstly calcined at 800 °C for 3 h. A second-calcination process was conducted at 950 °C for 6 h after sieving. After ball milling and sieving, the pressed pellets were sintered at 1550 °C in air for 3 h. Before the microstructure observations by scanning electron microscopy (SEM), the polished pellets were thermally etched at 1175 °C for 20 min. High temperature silver paste was applied on the two sides of pellets and dried at 600 °C for 20 min for the purpose of measuring dielectric properties. Crystallinity of GFI bulks was examined by X-ray diffraction analysis (XRD, Rigaku D/Max 2500, Japan). Surface morphologies of films were observed by scanning electron microscopy (SEM, Hitachi S-3500H, Japan). The energy dispersive spectroscopy (EDS) equipped on SEM was used to analyze the phase composition. Dielectric properties were measured with a precision impedance–capacitance–resistance meter (Model 4284A, Agilent Technologies, USA) at frequencies of 10^2 to 10^6 Hz. Leakage current was obtained by using an electrometer/high-resistance meter (Model 6517a, Keithley Instruments, Inc., USA).

3. Results and discussion

X-ray diffraction (XRD) patterns of $Gd(Fe_{1-x}In_x)O_3$ bulks are shown in Fig. 1. Pure $GdFeO_3$ bulk displayed as a single phase of the orthorhombic $GdFeO_3$-type perovskite with a random orientation. The substitution of 25% indium for Fe^{3+} kept the same structure as the pure $GdFeO_3$. The 25% solubility of indium in the Fe site was feasible for $GdFeO_3$ to form the solid solution of $Gd(Fe_{0.75}In_{0.25})O_3$ without a second phase. The GFI-0.5 bulk displayed a major $GdFeO_3$ structure but contained other phases to be identified. Pure $GdInO_3$ bulk also displayed a single phase of the hexagonal $GdInO_3$ perovskite with a random orientation. The $Gd(Fe_{0.25}In_{0.75})O_3$ bulk had the hexagonal $GdInO_3$ phase and other $GdFeO_3$-structure phases. For the GFI-0.25 bulk, diffraction peaks of the perovskite structure obviously shifted to a lower angle, indicating an increase in cell dimensions. The substitution of smaller Fe^{3+} [$r(Fe^{3+}) = 0.64$ Å of Ahrens ionic radius] with larger In^{3+} [$r(In^{3+}) = 0.81$ Å] is expected to expand the cell dimension and to lead to distortion caused by the dilated cells surrounded by the non-substituted cells [13]. On the other hand, the GFI-0.75 bulk showed an insignificant peak shift after substituting 25% Fe^{3+} for In^{3+}.

Fig. 2(a–c) shows the SEM images of 1550 °C-sintered GFI-x bulks for the indium contents at $x = 0$, 0.25, and 1.0. GFI-0, GFI-0.25, and GFI-1.0 displayed single-phase morphologies. The higher indium content led to a finer grain size. Pure $GdInO_3$ had a smallest grain size. The compositional analyses in each grain size coincided with their own formulated composition. No other second phases were detected. Surface morphology of the GFI-0.25 or $Gd(Fe_{0.75}In_{0.25})O_3$ bulk showed many small plates

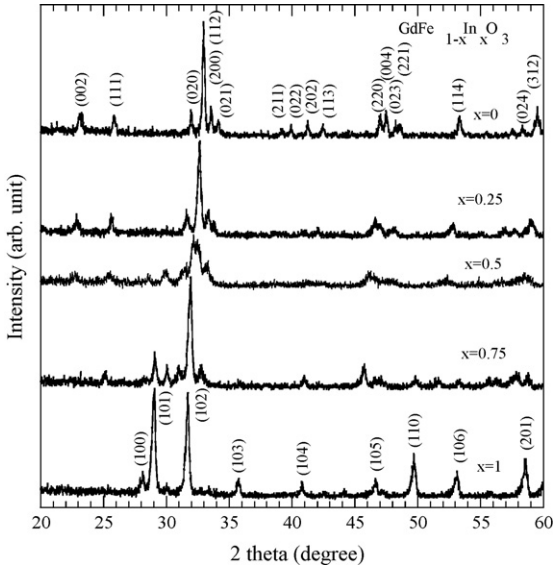

Fig. 1. X-ray diffraction patterns for 1550 °C-sintered $Gd(Fe_{1-x}In_x)O_3$ bulks with different indium contents.

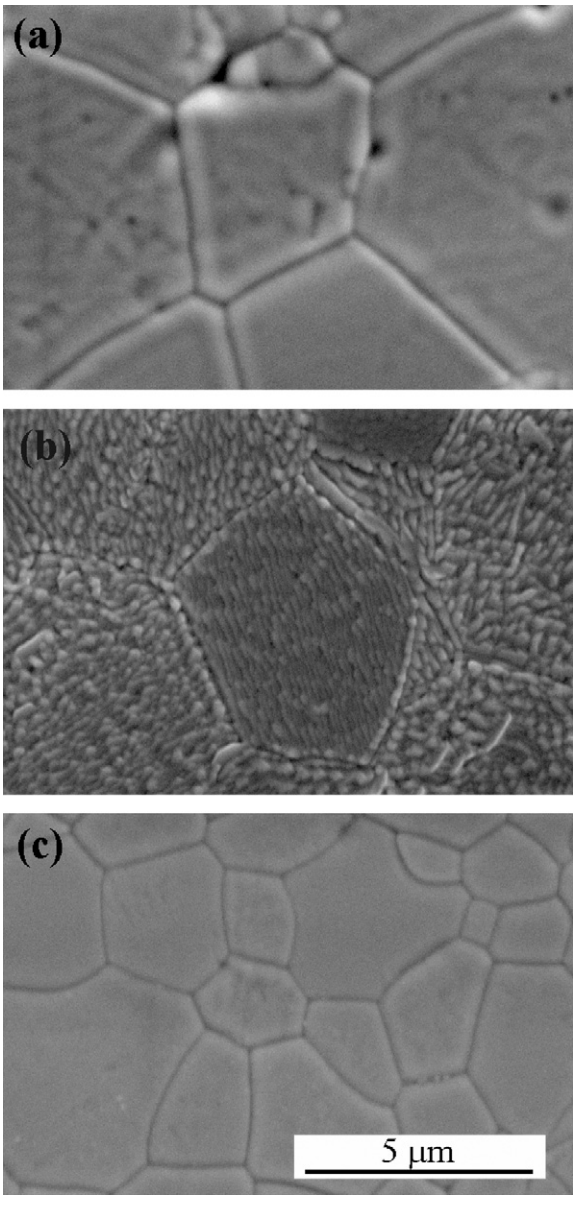

Fig. 2. SEM surface morphologies of 1550 °C-sintered $Gd(Fe_{1-x}In_x)O_3$ bulks with the indium contents at (a) $x = 0$, (b) $x = 0.25$, and (c) $x = 1.0$.

in each grain. These small plates can be related to anti-phases or electrical domains.

Fig. 3 displays the SEM image and the EDS element analysis of 1550 °C-sintered $Gd(Fe_{0.5}In_{0.5})O_3$ or GFI-0.5 bulk. The analysis at the (A) area obtained the element composition coincident with the formulated composition of $Gd(Fe_{0.5}In_{0.5})O_3$ or $Gd(Fe_{1/2}In_{1/2})O_3$. The element analysis at the (B) area with much more second phases had less Fe content and indicated the formation of Gd_5InO_9 or $5Gd_2O_3{\cdot}In_2O_3$. The element analyses at the (C) and (D) points, however, demonstrated the different distributions of Fe^{3+} and In^{3+} at the B site of ABO_3. It was the phase of $Gd(Fe_{1/3}In_{2/3})O_3$ with one third of the B sites occupied by Fe^{3+} and two thirds by In^{3+}.

Fig. 4 displays the SEM image and the EDS element analysis of 1550 °C-sintered $Gd(Fe_{0.25}In_{0.75})O_3$ or GFI-0.75 bulk. The analyses at the (B) area and the (D) point obtained the element composition coincident with the formulated composition of $Gd(Fe_{0.25}In_{0.75})O_3$ or $Gd(Fe_{1/4}In_{3/4})O_3$. The grain at the analysis (A) area did not exist the second phase. The element analysis at the (A) area indicated a Fe-less and In-rich phase with $GdInO_3$ as the major structure. The phase at the (A) area, therefore, was Fe-doped $GdInO_3$. The analysis at the (C) area identified the existence of the $Gd(Fe_{1/3}In_{2/3})O_3$ when the indium content in GFI was high.

Different phase compositions for the mixed $GdFeO_3$–$GdInO_3$ system were observed, which included $Gd(Fe_{3/4}In_{1/4})O_3$, $Gd(Fe_{1/2}In_{1/2})O_3$, $Gd(Fe_{1/3}In_{2/3})O_3$, and $Gd(Fe_{1/4}In_{3/4})O_3$. $GdFeO_3$ can dissolve up to 25% In^{3+} without forming second phases. For the formulated composition of $Gd(Fe_{0.5}In_{0.5})O_3$, some In^{3+}-rich $Gd(Fe_{1/3}In_{2/3})O_3$ phase can form accompanying by the formation of In^{3+}-less Gd_5InO_9 to maintain the mass balance. For the formulated composition of $Gd(Fe_{0.25}In_{0.75})O_3$ with much more the indium content, In^{3+}-less $Gd(Fe_{1/3}In_{2/3})O_3$ phase formed accompanying by the formation of In^{3+}-rich and Fe-doped $GdInO_3$ to maintain the mass balance. Therefore, the

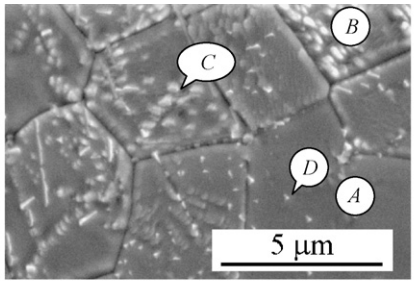

EDS element analysis				
Atomic % / site	Gd	Fe	In	O
(A) area	20.7	9.81	10.6	58.0
(B) area	33.8	0.38	7.33	58.5
(C) point	19.3	5.75	10.4	64.6
(D) point	18.6	6.77	10.4	64.2

Fig. 3. SEM surface morphology of 1550 °C-sintered $Gd(Fe_{0.5}In_{0.5})O_3$ bulks and its EDS element analyses at different area and points.

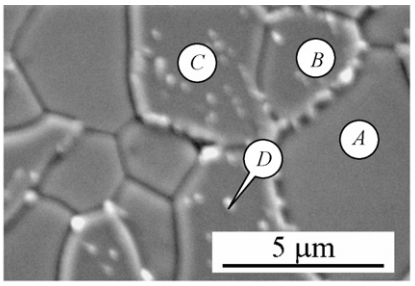

EDS element analysis				
Atomic % / site	Gd	Fe	In	O
(A) area	21.0	3.08	18.2	57.7
(B) area	20.9	4.76	15.3	59.1
(C) area	19.7	6.56	14.5	59.3
(D) point	19.0	4.78	13.3	62.9

Fig. 4. SEM surface morphology of 1550 °C-sintered $Gd(Fe_{0.25}In_{0.75})O_3$ bulks and its EDS element analyses at different area and points.

$Gd(Fe_{1/3}In_{2/3})O_3$ phase is a thermodynamically stable phase and can easily exist at the condition with a higher indium content at the B site of the ABO_3 structure.

Fig. 5 shows the variations of (a) the dielectric constant (ε_r) and (b) the dissipation factor ($\tan\delta$) with test frequency for $Gd(Fe_{1-x}In_x)O_3$ bulks with different indium contents. The ε_r values measured at 1 kHz and 1 MHz were 2485 and 50, 3680 and 120, 5070 and 50, 345 and 38, and 50 and 40 for GFI-x bulks with the indium contents at $x = 0$, 0.25, 0.5, 0.75, and 1.0, respectively. The $\tan\delta$ values measured at 1 kHz and 1 MHz

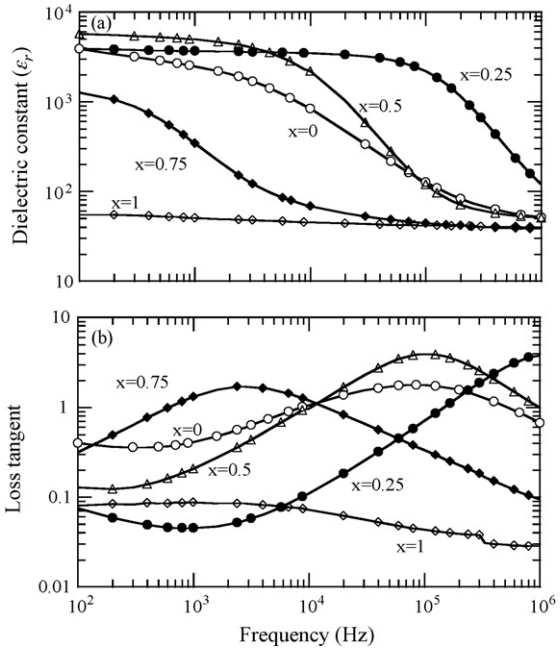

Fig. 5. The variations of (a) dielectric constant and (b) dielectric loss tangent with the test frequency for 1550 °C-sintered $Gd(Fe_{1-x}In_x)O_3$ bulks with different indium contents.

were 0.41 and 0.68, 0.05 and 3.86, 0.21 and 0.99, 1.31 and 0.09, and 0.09 and 0.03 for the GFI-x bulks with the indium contents at $x = 0$, 0.25, 0.5, 0.75, and 1.0, respectively. $GdInO_3$ remained frequency-independent with constant ε_r and low tan δ, while other compositions displayed a relaxation with a high → low ε_r change and a maximal loss peak at the resonance frequency (ω_r). This relaxation corresponds to the transition of dipolar polarization (lower frequency) to the ionic polarization (higher frequency). The ω_r values were 10^5, $\sim 10^6$, 1.2×10^5, and 2×10^3 Hz for GFI-x bulks with the indium contents at $x = 0$, 0.25, 0.5, and 0.75, respectively. Basically, the resonance frequency of $GdFeO_3$ should shift to lower frequency or the relaxation time take longer as the substitutes of In^{3+} have a heavier mass than Fe^{3+}. However, the addition of 25% In^{3+} shifted the resonance frequency more to higher frequency, indicating the response of dipolar polarization to the field frequency becomes faster. The special behavior for the 25% In^{3+}-added $GdFeO_3$ is attributed to the enhanced electrical polarization caused by the addition of larger ions to substitute Fe^{3+}, which leads to the dilation of unit cell (Fig. 1), lattice distortion, and enhanced polarization. For GFI-0.5 bulk, the contribution of enhanced polarization becomes less. For those with $x > 0.5$, they were dielectrics without enhanced polarization. That is to say, there is no dipolar polarization for $GdInO_3$ and GFI-0.75. Small plates in the grains of GFI-0.25 bulks (Fig. 2(b)) can be the evidence for the enhanced polarization.

Fig. 6 shows the variations of (a) the dielectric constant (ε_r) and (b) the dissipation factor (tan δ) with test temperature under a test frequency of 1 MHz for $Gd(Fe_{1-x}In_x)O_3$ bulks with different indium contents. ε_r reached a maximum with test temperature for the GFI bulks except for $GdInO_3$. $GdInO_3$ demonstrated temperature-stable characteristics in dielectrics. Up to 600 °C, ε_r of $GdInO_3$ remained constant and its loss

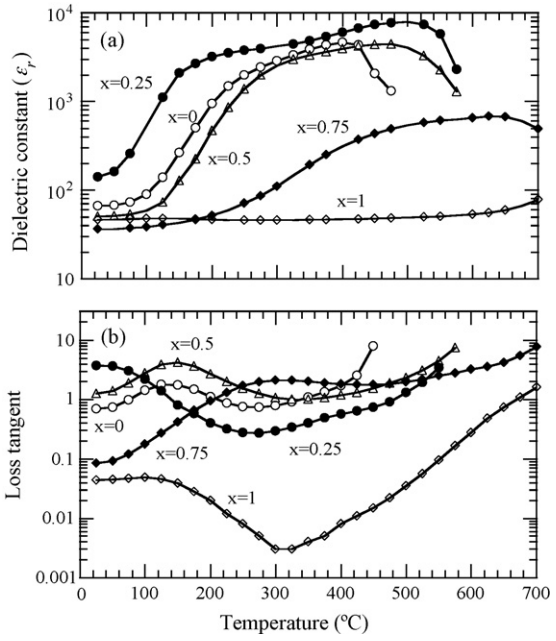

Fig. 6. The variations of (a) dielectric constant and (b) dielectric loss tangent with the measuring temperature for 1550 °C-sintered $Gd(Fe_{1-x}In_x)O_3$ bulks with different indium contents. The test frequency: 1 MHz.

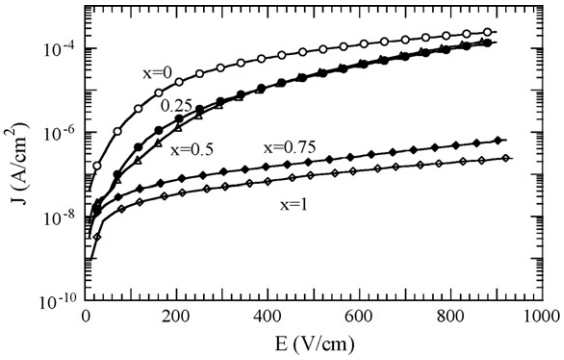

Fig. 7. The plot of log(leakage current density) vs. electric field for 1550 °C-sintered $Gd(Fe_{1-x}In_x)O_3$ bulks with different indium contents.

remained low. The maximal temperatures were 420, 520, 460, and 640 °C for GFI-x bulks with the indium contents at $x = 0$, 0.25, 0.5, and 0.75, respectively. After the maximal temperature, ε_r started to decrease, accompanying with a faster increase in tan δ. The variation of the maximal temperature with temperature for GFI-x bulks with different indium contents is in the same trend as the enhancement of polarization. The enhanced polarization for the 25% In^{3+}added $Gd(Fe,In)O_3$ led to the increase of Curie temperature from 420 to 520 °C, followed by lowering to 460 °C for the 50% In^{3+}-added $Gd(Fe,In)O_3$. Both of the GFI-0.75 and GFI-1.0 bulks, without the enhanced polarization, behaved like dielectrics and became leaky due to thermal activation at higher test temperatures above 600 °C.

Fig. 7 shows the variations of leakage current density and applied electric field in the form of log(J) versus E for GFI-x bulks at different indium contents. The addition of indium to $GdFeO_3$ improved the problem of leakage current. The resistivity measured at room temperature under 400 V cm^{-1} applied field was 6.8×10^6, 3.3×10^7, 3.3×10^7, 2.7×10^9 and 6.0×10^9 Ω cm for GFI-x bulks with the indium contents at $x = 0$, 0.25, 0.5, 0.75, and 1.0, respectively. At low applied dc field, all bulks had a linear dependence of log(J) versus $E^{1/2}$, which is identified as Schottky emission conduction, indicating the electrode/bulk interface controlled the dc conduction at low field. For the space charge-limited conduction with deep traps, it follows a power law relation, $J \propto E^m$ [14,15]. The J–E curves of GFI-0, GFI-0.25, and GFI-0.5, including the higher field part, can be fitted well with the modified Langmuir–Child law [16]:

$$J = aE + bE^2$$

with $a = 3.86 \times 10^{-8}$ Ω^{-1} cm^{-1} and $b = 2.63 \times 10^{-10}$ Ω^{-1} V^{-1} for $GdFeO_3$. This indicates that space charge-limited conduction is still dominant in the higher field region for GFI-0, GFI-0.25, and GFI-0.5 bulks. There is a transition from the Schottky emission (interface barrier) to space charge-limited (bulk barrier) conduction as the applied field increases. Oxygen vacancies have been related to the origin of space charges in some electronic ceramics [17]. The more oxygen vacancies, the more free carriers the bulks can create. The addition of In^{3+} into Fe^{3+} of $GdFeO_3$ leads to the decrease in the number of

oxygen vacancies and free carriers, which results in higher resistivity [10]. For GFI-0.75 and GFI-1.0, an exponential function, i.e., $\log(J) \propto E$, was observed, indicating that the conduction process is predominated by the field-assisted ionic conduction [14,15]. Therefore, the conduction mechanism can be changed from the space charge-limited conduction to the field-assisted ionic conduction as the indium content in $Gd(Fe,In)O_3$ becomes dominant. The occurrence of ionic conduction by ion species is attributed to the annihilation of oxygen vacancies. Therefore, the In^{3+} substitution for Fe^{3+} of $GdFeO_3$ can reduce the oxygen vacancies, favor the field-assisted ionic conduction, and lead to higher resistivity.

4. Conclusions

Orthorhombic $GdFeO_3$, hexagonal $GdInO_3$, and solid solutions of $Gd(Fe,In)O_3$ were sintered at 1550 °C and investigated. $GdFeO_3$ can dissolve 25% In^{3+} without forming the second phase. A stable product of $Gd(Fe_{1/3}In_{2/3})O_3$ was found in sintered bulks with formulated compositions of $Gd(Fe_{0.5}In_{0.5})O_3$ and $Gd(Fe_{0.25}In_{0.75})O_3$. Dielectric properties of the $GdFeO_3$–$GdInO_3$ system except $GdInO_3$ were quite frequency- and temperature-sensitive. The incorporation of In^{3+} into $GdFeO_3$ altered the dielectric and electrical properties. The resonance frequency increased up to 25% In^{3+} then decreased with further increasing the In^{3+} content. Combining with the microstructure observations of small plates in grains, the addition of 25% In^{3+} was expected to enhance polarization. The $Gd(Fe_{0.75}In_{0.25})O_3$ bulk had dielectric constant of 3680 and loss tangent of 0.045 under 1 kHz. $Gd(Fe_{1-x}In_x)O_3$ bulks with x not larger than 0.5 performed like ferroelectrics while behaved like dielectrics for those with $x > 0.5$. For those with compositions close to $GdInO_3$, $Gd(Fe,In)O_3$ bulks became stable in dielectrics and had lower leakage current. $Gd(Fe_{1-x}In_x)O_3$ bulks displayed a transition of space charge-limited conduction to the field-assisted ionic conduction as the indium content increased to annihilate oxygen vacancies.

Acknowledgement

We acknowledge the financial support by our National Science Council under Grant No. 95-2221-E-259-009-MY2.

References

[1] D. Treves, J. Appl. Phys. 36 (1965) 1033–1039.
[2] B. Lal, K.K. Bamzai, P.N. Kotru, B.M. Wanklyn, Mater. Chem. Phys. 85 (2004) 353–365.
[3] C. Li, Y. Thing, Y. Zeng, C. Wang, P.J. Wu, Phys. Chem. Solids 64 (2003) 2147–2156.
[4] P.M. Woodward, Acta Crystallogr. B53 (1997) 32–43.
[5] J. Wang, J.B. Neaton, H. Zheng, V. Nagarajan, S.B. Ogale, B. Liu, D. Viehland, V. Vaithyanathan, D.G. Schlom, U.V. Waghmare, N.A. Spaldin, K.M. Rabe, M. Wuttig, R. Ramesh, Science 299 (2003) 1719–1722.
[6] Y.H. Lee, C.S. Liang, J.M. Wu, Electrochem. Solid-State Lett. 8 (2005) F55–F57.
[7] Y.H. Lee, J.M. Wu, Y.L. Cheuh, L.J. Chou, Appl. Phys. Lett. 87 (2005) 172901.
[8] K. Ueda, H. Tabata, T. Kawai, Appl. Phys. Lett. 75 (1999) 555–557.
[9] J.K. Kim, S.S. Kim, W.J. Kim, A.S. Bhalla, R. Guo, Appl. Phys. Lett. 88 (2006) 132901.
[10] X. Qi, J. Dho, R. Tomov, M.G. Blamire, J.L. MacManus-Driscoll, Appl. Phys. Lett. 86 (2005) 062903.
[11] S.T. Zhang, Y. Zhang, M.H. Liu, C.L. Du, Y.F. Chen, Z.G. Liu, Y.Y. Zhu, N.B. Ming, Appl. Phys. Lett. 88 (2006) 162901.
[12] M.R. Levy, B.C.H. Steel, R.W. Grimes, Solid State Ionics 175 (2004) 349–352.
[13] R.D. Shannon, C.T. Prewitt, Acta Crystallogr. B25 (1969) 925–946.
[14] P.J. Horrop, Dielectrics, Butterworths, London, 1972, pp. 51–53.
[15] D.R. Lamb, Electric Conduction Mechanisms in Thin Insulating Films, Methuen, London, 1967.
[16] R.H. Tredgold, Space Charge Conduction in Solids, Elsevier, Amsterdam, 1966, pp. 75–79.
[17] J.F. Scott, C.A. Araujo, B.M. Melnick, L.D. McMillan, R.J. Zuleeg, Appl. Phys. 70 (1991) 382–388.